Analytical Methods

Accepted Manuscript

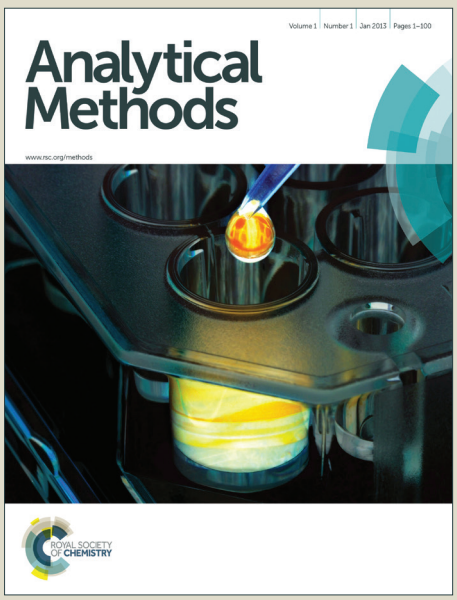

ROYAL SOCIETY OF CHEMISTRY

www.rsc.org/methods

Determination of arsenic by ICP-MS after retention on thoria nanoparticles

F.J. Pereira[a], M.D. Vázquez[b], L. Debán[b] and A.J. Aller[a,*]

[a]*Department of Applied Chemistry and Physics, Area of Analytical Chemistry; Faculty of Biological and Environmental Sciences, University of León, Campus de Vegazana, s/n, 24071 León, Spain; E-mail: aj.aller@unileon.es*

[b]*Department of Analytical Chemistry; Faculty of Sciences, University of Valladolid, C/Paseo de Belén, nº. 7, 47011 Valladolid, Spain*

ABSTRACT

A procedure for arsenic determination by ICP-MS in environmental and biological samples was developed using thoria nanoparticles for arsenic retention. Both inorganic arsenic species, $As^{(III)}$ and $As^{(V)}$, show similar behaviour regarding this thoria nanosorbent. The experimental data related to the amount of arsenic retained per gram of nanoparticles were theoretically modelled using mechanistic and empiric equations. The best kinetic theoretical relationship allowed us to obtain a feasible quantification of the retention process before reaching steady-state. In addition, calculation of the overall retention constant was also possible at steady-state. The maximum effective retention capacity for arsenic was about 30 mg As (g nanomaterial)$^{-1}$. The detection limit of the developed procedure was 0.07 μg As L^{-1} and the relative standard deviation 2.9%. The

accuracy of the developed procedure was assayed by the determination of arsenic in two certified reference materials.

Keywords: Arsenic; Thoria nanoparticles; Preconcentration; Mathematical modelling; Cysteine; Inductively coupled plasma – mass spectrometry

1. Introduction

Arsenic is a ubiquitous toxic element largely present in many environmental systems [1]. Arsenic can produce diverse adverse health effects in humans [2], also being considered as carcinogenic [3]. In ground water, arsenic exists almost exclusively as arsenite $\{As^{(III)}\}$ or arsenate $\{As^{(V)}\}$ for low and moderate/high redox potentials, respectively. These inorganic arsenic species are more toxic than the arsenic organic compounds. However, $As^{(III)}$ is much more toxic than $As^{(V)}$ due to its affinity for many essential enzymes in human metabolism [4]. Therefore, continued consumption of drinking water and foods containing even low levels of arsenic generates intoxication problems [5]. Consequently, monitoring of low levels of arsenic in the biological and environmental fields is of the greatest concern.

Different analytical techniques are usually employed for determination of arsenic, but in order to improve their analytical capabilities, isolation of low contents of arsenic from complex matrices are frequently used in combination. Isolation of arsenic has been largely assayed using the most common instrumental separation techniques, such as chromatography[6]. However, other separation methods for arsenic included the use of microorganisms as specific extractants, but particularly solid phase micro-

extraction [7, 8]. Different types of nanoparticles, mainly ceramic materials such as amorphous and crystalline titanium oxide [9-11], mixed magnetite–maghemite [12] , ceria [13], amorphous zirconium oxide[14], iron oxide[15, 16], and cupric oxide[17] have shown to be good sorbents for arsenic. These works studied the retention capabilities of uncapped-nanoparticles, being assisted by traditional isotherm models, but none analytical application was assayed. Other works, however, used nanoparticles based on different noble metals, particularly gold[18-21], silver[22], and platinum[23], for analytical purposes. Several determination techniques, including electrochemistry (anodic stripping voltammetry, cyclic voltammetry)[18, 21, 23, 24] and spectrometry (electrothermal atomic absorption spectrometry, spectrophotometry, colorimetry and ultrasensitive dynamic light scattering)[19, 20, 22, 25] were combined with a retention stage using nanoparticles for arsenic determination.

Taking advantage of the good capabilities of the solid extraction procedure, such as stability, easy handling, versatility and reusability, and our previous experience in the preparation and characterization of thoria-based nanoparticles[24, 26, 27], we want to develop a useful analytical tool for isolation of low contents of arsenic. On the other hand, additional advantages of any separation procedure can be raised if a theoretical model for the isolation procedure is derived. The mathematical modelling allows us to regulate and evaluate the modelled process without the necessity to realise any previous experiment. Modelling of arsenic retention by bacteria has already been assayed and adapted for analytical purposes [28, 29]. In this work, we present a theoretical one-site retention model, allowing quantitation of the amount of arsenic retained by the thoria nanoparticles. The aim of this work was to modify cysteine(Cyst)-capped thoria-based nanoparticles to be an efficient solid sorbent for arsenic. The arsenic retention process was followed measuring the amount of arsenic retained on the nanoparticle surface by

inductively coupled plasma – mass spectrometry (ICP-MS). After optimisation of the retention stage, an analytical procedure for the determination of inorganic arsenic species was developed. The environmentally relevant organoarsenic species, such as monomethylarsonate, dimethylarsenate, arsenobetaine, tetramethylarsonate, arsenosugars, etc., were not addressed in this study.

2. Theoretical considerations

From a theoretical point of view and assuming a one-site retention process, we can consider that the $As^{(III)}$ retention/desorption processes on the solid sorbent, Cyst-capped thoria nanoparticles (ThO_2-R-SH), are first-order processes, which can be represented in a simplified manner as follows

$$\mathbf{3ThO_2 - R - SH + As^{3+} \underset{k_d}{\overset{k_a}{\rightleftharpoons}} (ThO_2 - R - S)_3 - As + 3H^+}$$

where k_a and k_d are the retention and desorption rate constants, and R represents the radical HO_2C-$CH(NH_3^+)$-CH_2-. The k_a/k_d ratio is the overall retention constant, $\boldsymbol{K_r}$. The retention, v_a, and desorption, v_d, rates can be written

$$v_a = k_a C \quad (1)$$

$$v_d = k_d \beta \theta \quad (2)$$

We can consider the relationship between the molar concentration of the analyte in solution at any time, *C,* and the initial molar concentration of the analyte in solution, C_o,

$$C = C_o - \beta\theta \quad (3)$$

where θ is the retained analyte fraction ($0 \leqslant \theta \leqslant 1$) at any time from the maximum retention capacity, q_m. This last parameter can be expressed in concentration units as $\beta = \frac{m_s q_m}{M_w V}$, where m_s is the sorbent mass, M_w is the molecular mass of the analyte and V

is the sample volume. Taking in consideration these parameters, Eq. (1) can be rewritten as follows

$$v_a = k_a(C_o - \beta\theta) \quad (4)$$

The overall rate of the $As^{(III)}$ retention process is

$$\frac{d\theta}{dt} = v_a - v_d = k_a(C_o - \beta\theta) - k_d\beta\theta \quad (5)$$

For a fixed initial molar concentration of the analyte, C_o is constant. Thus, rearranging and integrating Eq. (5) with the following boundary conditions ($t = 0,\ \theta = 0$ and $t = t,\ \theta = \theta$), we obtain the corresponding integrated equation

$$\frac{1}{(-k_a - k_d)\beta}\, log(k_a C_o + (-k_a - k_d)\beta\theta)\Big|_{0}^{\theta} = t|_{0}^{t} \quad (6)$$

Replacing the value of $\beta\theta$ from Eq. (3) and making operations, we arrive to

$$(C_o - C) = \left(\frac{k_a C_o}{k_a + k_d}\right)\left(1 - e^{-(Ln10)(k_a + k_d)\beta t}\right) \quad (7)$$

The term C_o-C is a measure of the amount of arsenic retained expressed in concentration units at any time, and it can be accordingly replaced by the amount of arsenic retained per mass unit of sorbent, q, before reaching steady-state. In this case, Eq. (7) is generalised as follows,

$$q = a\left(1 - e^{-b\,t}\right) \quad (7')$$

where a (μg g^{-1}) and b (μmol L^{-1} min^{-1}) would be two constants dependent on the parameters k_a, k_d, C_o, and β. Eq. (7) can be rewritten for very short retention times, following Taylor's series transformations,

$$C_o - C = 2.3\,\beta k_a C_o t \quad (8)$$

where C_o-C in Eq. (8) refers to the amount of $As^{(III)}$ retained by the thoria nanoparticles before reaching steady-state. Eq. (8) allows us to perform a quantitative analysis long before the retention equilibrium is reached. Check please that Eq. (8) can also be used to model the amount of arsenic retained as a function of the initial arsenic concentration, C_o, for a fixed retention time.

For very long retention times, the steady-state situation is always reached, which can be analytically characterized by the partitioning equilibrium constant. Once the retention process has reached steady-state, the retention equilibrium is achieved and the left hand in Eq. (5) would be null, $\frac{d\theta}{dt} = 0$, while $\theta = \theta_e = 1$, and $C = C_e$. Consequently, Eq. (5) can be rewritten as

$$0 = k_a C_o - k_a \beta - k_d \beta \qquad (9)$$

Considering the overall retention constant, $\boldsymbol{K_r} = \frac{\boldsymbol{k_a}}{\boldsymbol{k_d}}$, and replacing the value of β from Eq. (3) for the retention equilibrium, where $\theta_e = 1$, in the second term of the right hand of Eq. (9), we can obtain after rearrangements

$$\boldsymbol{C_o - C_e = K_r C_e} \qquad (10)$$

A plot of $C_o - C_e$ vs. C_e for several values of C_o allow us to obtain, from the slope of the straight line plotted, the value of the overall retention constant, $\boldsymbol{K_r}$.

3. Experimental

3.1. Instruments and operating conditions

Inductively coupled plasma mass spectrometry (ICP-MS) with an octopole reaction system ICP-MS operated in a He/H_2 cell mode (HP 7500c, Agilent, Tokyo, Japan) was

used for all measurements of arsenic. The sample solutions were pumped by an ASX 500 model 510 auto-sampler (Cetac Technologies, Omaha, NB, USA). Further details of the instrumental settings are given in Table 1. The mass-scanning data acquisition mode was used for optimization and a mixed internal-standard solution (5 μg L^{-1}) of ^{74}Ge and/or ^{89}Y was used to correct short-term drift. Separation and quantification of $As^{(III)}$ and $As^{(V)}$ were performed using HPLC-ICP-MS. The instrument settings were checked daily.

The HP 1100 HPLC system series 1260 Infinity with a manual pump Agilent 61310 *Iso pump* (Agilent Technologies, USA) was used for separation of $As^{(III)}$ and $As^{(V)}$. An anion exchange column (G3154-65002: guard column, Agilent) was used for arsenic speciation. The HPLC parameters used throughout the experiments were 10^{-6} bar pressure, 1 mL min^{-1} mobile phase flow and 100 μL sample volume. Composition of the mobile phase was 2.0 mmol L^{-1} sodium phosphate plus 0.2 mmol L^{-1} EDTA at pH 6.0.

Temperature was controlled by a digital dry bath (Labnet International D1100) (Edison, NJ, USA). All experiments were carried out at room temperature. The acidity of the aqueous phase was measured, when necessary, with a pH-meter (Crison model Digit 505) (Barcelona, Spain). Chemicals and nanoparticles (dry weight) were weighted on a Mettler AE 240 semi-microanalytical balance (sensitivity ±0.01 mg) (Mettler-Toledo S.A.E., Barcelona, Spain). A centrifuge Digicen 20 (Orto Alresa, Madrid, Spain) was used at 9000 rpm for 30 min to separate the precipitate at room temperature.

3.2. Chemicals and reagents

Arsenite and arsenate stock solutions (1000 mg L^{-1}) were prepared by dissolving suitable amounts of sodium arsenite and *di*-sodium hydrogen arsenate (Merck, Darmstadt, Germany) in appropriate volumes of distilled, deionized water (18 MΩ cm). Standard stock solutions (10000 mg L^{-1}) of the other elements studied as interferents were prepared from their salts (nitrate, when possible) by a conventional method. Working solutions were prepared daily prior to their use. All chemicals were of analytical reagent grade (Merck) and used without further purification. The pH of the aqueous solutions was adjusted with 0.1 mol L^{-1} HNO_3 and 0.1 mol L^{-1} NaOH solutions. Blank solutions for ICP-MS measurements were prepared using the appropriate nanoparticles submitted to exactly the same separation/preconcentration procedure but without arsenic species.

3.3. Preparation of Cyst-capped thoria nanoparticles and other sorbents

We prepared three types of ThO_2-based nanoparticles: ThO_2-, Cyst-capped ThO_2-, and Cyst-adsorbed ThO_2-based nanoparticles. Cyst-capped thoria nanoparticles were prepared adapting the procedure developed elsewhere [26]. $Th^{(IV)}$ (0.02 mol L^{-1}) was mixed together with *l*-cysteine (0.25 mol L^{-1}) aqueous solution at pH 8.0, degassed with N_2 and in the presence of up to 5 mol L^{-1} 1,2-ethanediol to favour precipitation of the solid phase. The precipitate was separated by centrifugation, washed three times with an aqueous solution at pH 8.0 and dried at 348 K. The average nanoparticle size was below 20 nm. Pure ThO_2 nanoparticles were precipitated in a similar manner as the Cyst-capped ThO_2 nanoparticles but in the absence of *l*-cysteine. To prepare Cyst-adsorbed ThO_2 nanoparticles, pure ThO_2 nanoparticles were put in contact with a 0.25 mol L^{-1} Cyst solution at pH ~8.0 for 30 min. Then, the Cyst-adsorbed ThO_2 nanoparticles were poured from the supernatant.

3.4. Procedure for $As^{(III)}$ retention/determination

A 25 mg (or as indicated) weight of Cyst-capped thoria nanoparticles was added to the sample solution (10 mL) at pH 8.0±0.2 for retention times of 1–10 min (or as indicated) at room temperature. The slurry was separated by centrifugation, washed twice with 5 mL of basic water at pH ~8.0. The thoria nanoparticles with the arsenic retained were treated with 0.2 mL of 70% nitric acid at room temperature, diluted with 0.1 mol L^{-1} nitric acid to bring each sample to the final volume (10 mL) and the amount of arsenic measured by ICP-MS. When necessary, the amount of arsenic present in the supernatant was also measured by ICP-MS, also treating the supernatant with 70% nitric acid. The included experimental data represent the mean of three independent assays.

3.5. Standard Reference Materials (SRM) preparation

Air-dried National Institute of Standards and Technology (NIST) SRM 1633a coal fly ash samples were prepared as elsewhere with minor modifications[29]. The sample pH was adjusted to 8.0±0.2 using NaOH, with sufficient sodium tartrate added so as to avoid precipitation as hydroxides of the main matrix elements. Air-dried SRM 1568a rice flour samples were also prepared as elsewhere [30] and the sample pH was also adjusted as before. Spiking studies with the NIST materials were carried out by treating the solid samples with different amounts of $As^{(III)}$ standard solutions prior to the dissolution procedure. Measurements were calibrated either by treating the $As^{(III)}$ standards in the same way as the samples via nanoparticle pre-concentration, or by directly using $As^{(III)}$ standard aqueous solutions.

4. Results and discussion

4.1. Selection of the nanomaterial

To obtain an adequate solid sorbent for $As^{(III)}$, various thoria-based nanoparticles were compared for arsenic isolation (Fig. 1). As stated in Fig. 1, the highest efficiencies in the retention of $As^{(III)}$ were obtained for the Cyst-capped thoria nanoparticles followed by the Cyst-adsorbed thoria nanoparticles. The developed thoria-based nanoparticles accumulated up to 10-fold more $As^{(III)}$ than the zirconia-based nanoparticles prepared in similar ways (Fig. 1). In the following, we only used Cyst-capped thoria nanoparticles.

The effect of the time lag between the precipitation and isolation of the Cyst-capped thoria nanoparticles on the retention of $As^{(III)}$ was also evaluated. The amount of $As^{(III)}$ retained by the Cyst-capped thoria nanoparticles decreased for growing time lags in the range 0 - 20 days, as measured by ICP-MS. This is probably due to the fact that the nanoparticles evolve strongly with time when in contact with the original sample solution, particularly increasing their crystallite sizes and consequently decreasing the surface/volume ratio. In conclusion, Cyst-capped thoria nanoparticles were always isolated from the supernatant immediately (less than 5 min) after their precipitation. The prepared sorbent was stable (variability <5%) for at least one month on storing.

4.2. Optimization of the retention conditions

Firstly, we optimized the amount of cysteine used for capping the thoria nanoparticles. Fig. 2 shows that the $As^{(III)}$ retention increased strongly with the cysteine concentration used for capping the ThO_2 nanoparticles but, above 0.1 mol L^{-1} cysteine solutions, the amount of the $As^{(III)}$ retained was constant. However, to assure a good capping process, 0.25 mol L^{-1} cysteine solutions were always used for all experiments.

The sample solution pH may affect the retention capacity of many solid sorbents. The capacity of the Cyst-capped thoria nanoparticles for $As^{(III)}$ retention was greatly improved at slightly basic pHs (Fig. 3), selecting the pH 8.0 as an optimal value.

However, pH variation was noted during the retention process and Fig. 3 shows the initial and final pH values obtained during $As^{(III)}$ retention. This pH variation was generated by the ThO_2 nanoparticles itself which suffer a hydrolysis reaction when in contact with aqueous solutions at the working pH (Fig. S1A). Extension of the hydrolysis reaction was dependent on the weight of nanoparticles (Fig. S1B) and the retention time (Fig. S1C), but not on the amount of $As^{(III)}$ (Fig. S1D), at least notably in the $As^{(III)}$ concentration range assayed. The small pH variation supported by the Cyst-capped ThO_2 nanoparticles (Fig. S1B) against the uncapped-ThO_2 nanoparticles is an additional indication that cysteine was bound to the ThO_2 nanoparticle surface through the oxygen atoms of the carboxylic group, matching the behaviour of the OH^- groups originated from water dissociation. We assayed the effect of three ligands (EDTA, fluoride and tartrate) on the pH variation during the $As^{(III)}$ retention process, but better results were found using tartrate, as the final pH was ~7.5 for any basic initial pH. No buffered solutions were used to avoid, as far as possible, very complex matrices. However, tartrate was present to elude precipitation and retention of any concomitant metal, such as $Al^{(III)}$ and $Fe^{(III)}$, because of its maximum efficiency as a masking in the pH range 7.0 – 8.0, as it is fully deprotonated (Fig. S2). The $As^{(III)}$ retention process itself really occurs with no pH variation (Fig. S1D), what is explained on the basis of a maximum protonation of the thiol (-SH) group of cysteine (Fig. S2) at the pH generated after hydrolysis of the Cyst-capped ThO_2 nanoparticles. Under these neutral pH conditions, the $As^{(III)}$ hydroxylated species, $As(OH)_3$, predominate in solution (pK_a = 9.1, 12.13, and 13.4) (Fig. S2), thus facilitating the $As^{(III)}$ retention process.

Other parameters, such as the weight of the Cyst-capped ThO_2 nanoparticles (Fig. 4) and the contact time of the arsenic-retaining nanoparticles with a nitric acid solution before ICP-MS measurements, were also evaluated. Fig. 4A shows that the

amount of arsenic retained strongly increased with the weight of nanoparticles up to 25 mg, but above this value, the amount of $As^{(III)}$ retained was constant. This saturation in the retention of $As^{(III)}$ is regulated by both the sample volume and the $As^{(III)}$ concentration used. Fig. 4B shows the amount of $As^{(III)}$ retained per gram of nanoparticle, q, as a function of the weight of nanoparticles. The values of q decrease strongly with the weight of nanoparticles, but above 25 mg of nanoparticles, the retention (q value) tends to be stabilized. On the other hand, the effect of the contact time between the arsenic-retaining nanoparticles and a nitric acid solution before ICP-MS measurements of arsenic was particularly noted for very short time values, while after a contact time of about 10 minutes, the amount of $As^{(III)}$ measured was constant.

4.3. Modelling of $As^{(III)}$ retention

4.3.1. Kinetics. Fig. 5 shows the $As^{(III)}$ retention-time profile with an initial stage covering the first initial 10 min, where the amount of $As^{(III)}$ retained increased rapidly. During a second stage, from 10 to 120 min (Fig. 5), the amount of $As^{(III)}$ retained increased more slowly, eventually reaching a pseudo-equilibrium, probably regulated by the existence of a simultaneous desorption process. The derivative plot (the inset in Fig. 5) confirms this conclusion, because the retention rate is very high during the early stage of the retention process, but above 10 min it takes very small constant values.

The amount of $As^{(III)}$ retained by the Cyst-capped thoria nanoparticles as a function of time was theoretically modelled using Eq. (7'). Eq. (7') is a mechanistic equation fitting well the experimental kinetic data (Table 2). However, according to the coefficient of determination value, a better fitting was followed using Monod-type kinetics (empirical model) (Table 2), where q (μg g^{-1}) is the amount of $As^{(III)}$ retained per mass unit of sorbent at any time, q^t_m (μg g^{-1}) is the maximum amount of $As^{(III)}$

retained per mass unit of sorbent, $t_{1/2}$ (min) is the half-retention time corresponding to the half-retention amount, and t (min) is the retention time (Table 2). This kinetics behaviour suggests a probable redox catalytic retention process. The half-retention time was very short, indicating that the retention kinetics is very rapid. This allows us to derive a quantitative relationship, similar to Eq. (8), between the amount of $As^{(III)}$ retained and time before the retention equilibrium is reached. Using a fixed initial $As^{(III)}$ concentration of 200 μg L^{-1}, the experimental retention data obtained in the time interval of 0-10 min fit well to the following straight line, $q = (13.1\pm3.0)t$ (r^2 = 0.98207).

4.3.2. Retention equilibrium. The amount of $As^{(III)}$ retained by the Cyst-capped thoria nanoparticles for a fixed retention time was firstly related to the initial $As^{(III)}$ concentration in the sample solution, C_o, as it is more attractive from an analytical point of view. Fig. S3 shows that $As^{(III)}$ retention follows a two-step process, in which the amount of $As^{(III)}$ retained grown very rapid at lower initial $As^{(III)}$ concentrations. Mathematical modelling of this retention process was also followed using mechanistic, Eq. (7'), and empirical hyperbolic equations. Very similar fittings were obtained with both equations, although the hyperbolic equation provided a higher coefficient of determination (Table 3). The maximum amounts of $As^{(III)}$ retained per mass unit (dry weight) of nanoparticles were similar for both models (Table 3). For $As^{(III)}$ concentrations below $C^o_{1/2}$, a theoretical equation similar to Eq. (8) can be derived. It was found that the amount of $As^{(III)}$ retained per mass unit of nanoparticle [q, in mg As (g nanoparticle)$^{-1}$] increased linearly, $q = (0.50\pm0.00)C_o$ (r^2 = 0.99938), with the initial $As^{(III)}$ concentrations (C_o, mg L^{-1}) in the range 0–25 mg L^{-1} for a fixed retention time of 10 min. This relationship can be used for analytical purposes because of the direct

relationship between the amount of $As^{(III)}$ retained and the initial $As^{(III)}$ concentration in the sample solution.

To correlate the amount of $As^{(III)}$ retained with the $As^{(III)}$ concentration at equilibrium in the sample solution (supernatant) for a fixed small retention time, we used a hyperbolic model, similar to the Langmuir plot, allowing determination of the theoretical retention capacity, q_m, at saturation (Table 4). Furthermore, the equilibrium constant, I_L (L mol^{-1}), for the Langmuir model, can be used to calculate the Gibbs free energy of the $As^{(III)}$ retention process. The values found for the thermodynamic parameters (Table 4) are indicative of a spontaneous retention process.

The related dimensionless retention constant, $\boldsymbol{K}_r$, introduced in the theoretical section, Eq. (10), took the value (27.8 ± 0.8) (r^2 = 0.98904), what means that the retention of arsenic is largely favoured under the conditions used. Alternatively, the distribution coefficient (partitioning equilibrium constant, K_D) of $As^{(III)}$ for the retention system involved, Cyst-thoria nanoparticles / aqueous solution, allow us also to evaluate the amount of $As^{(III)}$ retained at equilibrium. The K_D parameter fit well the following equation, $K_D = (26.2 \pm 1.6) \exp(-C_e/(0.23 \pm 0.06))$ (r^2 = 0.97089), as a function of the $As^{(III)}$ concentration at equilibrium (C_e, μg L^{-1}).

4.4. Analytical applications

The analytical characteristics of the developed procedure were obtained under the selected optimal conditions. The linear $As^{(III)}$ concentration range was established near the limit of detection up to at least 25 mg L^{-1}, as stated in the previous section, which accounts for a very wide working range. The lower limit of detection was found to be 0.07 μg L^{-1} (3σ), which compares favourably with those previously reported methods

using nanosorbents for the isolation of inorganic arsenic species[19,22,25,29,31-35] and spectrometric and electrochemistry techniques for detection. However, other works have provided slightly improved limits of detection for the same inorganic arsenic species in water samples,[36-38] but particularly better improvements were found in those methods including hyphenated techniques where separation and pre-concentration stages, usually achieved by high performance liquid chromatography (HPLC) and hydride generation (HG), were coupled with ICP-MS[39-48] (Table 5). Notwithstanding, the limit of detection obtained in this work shows enough sensitivity to be used in any practical determination of the inorganic arsenic species in complex matrices. On the other hand, any comparison between limits of detection suffers from some weaknesses because the detection limit value largely depends on the detector used, as well as on the composition of the blank solution, not always standardised. Furthermore, additional inconsistencies for an accurate general comparison between the analytical methods derived from the different criteria and/or statistical conditions established by the authors for calculation of the limits of detection (Table 5). The precision (relative standard deviation) for 10 replicate determinations at 100 μg $As^{(III)}$ L^{-1} was 2.9%. The theoretical maximum retention capacity was established at nearly 30 mg As (g nanoparticle)$^{-1}$.

The effect of several ions, $Al^{(III)}$, $Ca^{(II)}$, $Cd^{(II)}$, $Co^{(II)}$, $Cr^{(VI)}$, $Cu^{(II)}$, $Fe^{(III)}$, $Hg^{(II)}$, $K^{(I)}$, $Mg^{(II)}$, $Mn^{(II)}$, $Na^{(I)}$, $Ni^{(II)}$, $Pb^{(II)}$, $Sb^{(III)}$, $Sb^{(V)}$, $Si^{(IV)}$, $V^{(V)}$, $Zn^{(II)}$ and chloride, on the retention of $As^{(III)}$ (50 mg L^{-1}), in the presence of tartrate as a masking, was evaluated. No interferences (<5%) were found when present up to 50 mg L^{-1}, what is in agreement with the smaller and higher conditional formation constants for these elements when joined to cysteine and tartrate, respectively, as compared with the corresponding one for $As^{(III)}$ [49]. A few of these ions {particularly $Cu^{(II)}$ and $Hg^{(II)}$} show some minor interfering

effects when present at higher concentrations. However, the potential interferent effects were largely solved by controlling the amount of tartrate added.

Looking for potential speciation analysis of the inorganic arsenic species, the capability of the developed nanomaterial to retain $As^{(V)}$ was also evaluated. To check the retention of $As^{(V)}$, a solution containing different amounts of $As^{(V)}$ and several mixtures of $As^{(III)}$ plus growing amounts of $As^{(V)}$ were treated with the nanoparticles. After the retention process, the nanoparticles were separated from the supernatant and washed with water at the retention pH. The total amount of arsenic present in both nanoparticles and water solutions was determined by ICP-MS, while the amounts of $As^{(III)}$ and $As^{(V)}$ present in the wash solutions were evaluated by HPLC-ICP-MS. The presence of $As^{(V)}$ shown some effect on the retention of $As^{(III)}$, because the $As^{(V)}$ ion was also quantitatively retained by the Cyst-capped thoria nanoparticles in a similar way as the $As^{(III)}$ ions do. In other words, the plot of the amount of $As^{(V)}$ retained versus the $As^{(V)}$ present in the sample solution growth linearly with a slope statistically similar to that obtained using $As^{(III)}$. On the other hand, $As^{(V)}$ was found no present in the wash solutions. Fig. 6 shows typical chromatograms obtained from solutions containing mixtures of $As^{(III)}$ and $As^{(V)}$ standards at low levels (Fig. 6A) and flat chromatograms obtained from the wash solutions (Fig. 6B). Results from Fig. 6 are clear indication that the $As^{(V)}$ ions were bound to the nanoparticles.

The retention mechanism for $As^{(III)}$ was stablished above as a result of a complexation process with the sulfhydryl group of cysteine. However, it is not clear how $As^{(V)}$ was retained by cysteine. The $As^{(V)}$ ions mainly react with reduced nitrogen groups such as amines, but not with sulfhydryl groups. Nonetheless, this retention mechanism is not probable because nitrogen in cysteine is largely protonated under the pH conditions used. Alternatively, a more plausible mechanism for the retention of

$As^{(V)}$ would be related to a catalytic reduction process of $As^{(V)}$ to $As^{(III)}$ by cysteine. This organic molecule has already been largely used for this purpose[50,51]. In any case, since all two arsenic species give the same response, a single arsenic species can be used for calibration. Consequently, the developed procedure can also be used to determine the total amount of arsenic $\{As^{(III)} + As^{(V)}\}$ without any previous redox manipulation of the sample solution. Furthermore, many acidic treatments of the solid samples generate only the $As^{(III)}$ ions in solution.

The feasibility of the developed procedure was tested using two certified reference materials, coal fly ash (NIST SRM 1633a) and rice flour (NIST SRM 1568a). The values found for the arsenic content in the NIST standard reference materials were in agreement with the certified values (Table 6) according to a Student *t*-test at a 95% confidence level. The recovery of arsenic from both the artificial samples and the standard reference materials (Table 6) was between 97.7% and 103.5%, demonstrating the validity and accuracy of the developed procedure.

5. Conclusions

It was clearly shown that, under the established conditions, the Cyst-capped thoria nanoparticles can act as a good sorbent for $As^{(III)}$ and $As^{(V)}$, showing excellent capabilities to be used in removing large amounts of the inorganic arsenic species from polluted aqueous samples. It is remarkable that this sorbent shows similar behaviour against retention of $As^{(III)}$ and $As^{(V)}$. The new procedure allowed the accurate determination of arsenic in complex samples by ICP-MS with no matrix effect. From a theoretical point of view, the retention kinetics and equilibrium data were better modelled using hyperbolic functions. Nonetheless, linear models for earlier stages of the retention process and low arsenic concentrations were also theoretically derived. In

addition, the overall retention constant of the arsenic retention process was obtained for the steady-state situation.

Acknowledgements A Contract from the Junta de Castilla y León, Consejería de Cultura, and Fondo Social Europeo was awarded to one of the authors (FJP) and is gratefully acknowledged.

References

1 P. Bhattacharya, A. H. Welch, K. G. Stollenwerk, M. J. McLaughlin, J. Bundschuh and G. Panaullah, *Sci. Total Environ.,* 2007, **379**, 109-120.

2 K. F. Akter, G. Owens, D. E. Davey and R. Naidu, *Rev. Environ. Contam. Toxicol*., 2005, **184**, 97-149.

3 K. T. Kitchin, *Toxicol. Appl. Pharmacol.,* 2001, **172**, 249-261.

4 B. K. Mandal and K. T. Suzuki, *Talanta,* 2002, **58**, 201-235.

5 U.S. Environmental Protection Agency, *www. epa. gov/safewater/arsenic. html1,* 2007.

6 Y. Morita, T. Kobayashi, T. Kuroiwa and T. Narukawa, *Talanta,* 2007, **73**, 81-86.

7 C. Yu, Q. Cai, Z. Guo, Z. Yang and S. B. Khoo, *Spectrochim. Acta Part B: At. Spectrosc.,* 2003, **58**, 1335-1349.

8 S. Chen, X. Zhan, D. Lu, C. Liu and L. Zhu, *Anal. Chim. Acta,* 2009, **634**, 192-196.

9 G. Jegadeesan, S. R. Al-Abed, V. Sundaram, H. Choi, K. G. Scheckel and D. D. Dionysiou, *Water Res.,* 2010, **44**, 965-973.

10 H. Jezequel and K. Chu, *J. Environ. Sci. Health Part A,* 2006, **41**, 1519-1528.

11 H. Sun, X. Zhang, Z. Zhang, Y. Chen and J. C. Crittenden, *Environ. Poll.,* 2009, **157**, 1165-1170.

12 S. R. Chowdhury and E. K. Yanful, *J. Environ. Manage.,* 2010, **91**, 2238-2247.

13 Q. Feng, Z. Zhang, Y. Ma, X. He, Y. Zhao and Z. Chai, *Nanoscale Res. Lett.,* 2012, **7**, 1-8.

14 H. Cui, Q. Li, S. Gao and J. K. Shang, *J. Ind. Eng. Chem.,* 2012, **18**, 1418-1427.

15 S. Luther, N. Borgfeld, J. Kim and J. Parsons, *Microchem. J.,* 2012, **101**, 30-36.

16 W. Tang, Q. Li, S. Gao and J. K. Shang, *J. Hazard. Mater.,* 2011, **192**, 131-138.

17 C. A. Martinson and K. Reddy, *J. Coll. Interf. Sci.,* 2009, **336**, 406-411.

18 X. Dai, O. Nekrassova, M. E. Hyde and R. G. Compton, *Anal. Chem.,* 2004, **76**, 5924-5929.

19 S. Gunduz, S. Akman, A. Baysal and M. Culha, *Microchim. Acta,* 2011, **172**, 403-407.

20 J. R. Kalluri, T. Arbneshi, S. Afrin Khan, A. Neely, P. Candice, B. Varisli, M. Washington, S. McAfee, B. Robinson and S. Banerjee, *Angew. Chem.,* 2009, **121**, 9848-9851.

21 E. Majid, S. Hrapovic, Y. Liu, K. B. Male and J. H. Luong, *Anal. Chem.,* 2006, **78**, 762-769.

22 S. Gunduz, S. Akman, A. Baysal and M. Kahraman, *Spectrochim. Acta Part B: At. Spectrosc.,* 2010, **65**, 297-300.

23 S. Sanllorente-Méndez, O. Domínguez-Renedo and M. J. Arcos-Martínez, *Electroanalysis,* 2009, **21**, 635-639.

24 F. J. Pereira, M. D. Vázquez, L. Debán and A. J. Aller, *Electrochim. Acta,* 2013, **109**, 125-135.

25 K. Morita and E. Kaneko, *Anal. Chem.,* 2006, **78**, 7682-7688.

26 F. J. Pereira, M. T. Díez and A. J. Aller, *J. Nanopart. Res.,* 2013, **15**, 1-12.

27 F. J. Pereira, M. D. Vázquez, L. Debán and A. J. Aller, *Polyhedron,* 2014, **76**, 71-80.

28 E. Ordoñez, A. F. Villadangos, M. Fiuza, F. J. Pereira, J. A. Gil, L. M. Mateos and A. J. Aller, *Environm. Chem.,* 2012, **9**, 121-129.

29 A.F. Villadangos, E. Ordóñez, M. Muñoz, I. Pastrana, M. Fiuza, J.A. Gil, L.M. Mateos and A.J. Aller, *Talanta,* 2010, **80**, 1421-1427.

30 L. Robles and A.J. Aller, *Talanta,* 1995, **42**, 1731-1744.

31 L. Xiao, G.G. Wildgoose, R.G. Compton, *Anal. Chim. Acta*, 2008, **620**, 44–49.

32 Y.C. Sun, Y.J. Chen, Y.N. Tsai, *Microchem. J.,* 2007, **86**, 140–145.

33 Yue-Shian Song, Govindan Muthuraman, Yi-Zhen Chen, Chu-Chieh Lin and Jyh-Myng Zen, *Electroanalysis*, 2006, **18**, 1763-1770.

34 A.O. Simm, C.E. Banks, Sh.J. Wilkins, N.G. Karousos, J. Davis, R.G. Compton, *Anal. Bioanal. Chem*., 2005, **381**, 979–985.

35 S. Londesborough, J. Mattusch, R. Wennrich, *Fresenius J. Anal. Chem.,* 1999, **363**, 577–581.

36 D. Li, J. Li, X. Jia, Y. Han, E. Wang, *Anal. Chim. Acta*, 2012, **733**, 23–27.

37 I. López-García, R.E. Rivas, M. Hernández-Córdoba, *Talanta,* 2011, **86**, 52-57.

38 K. Gibbon-Walsh, P. Salaün, C.M.G. van den Berg, *Anal. Chim. Acta*, 2010, **662**, 1–8.

39 G. Raber, N. Stock, P. Hanel, M. Murko, J. Navratilova, K.A. Francesconi, *Food Chem.,* 2012, **134**, 524–532.

40 Á.H. Pétursdóttir, H. Gunnlaugsdóttirm, H. Jörundsdóttir, A. Mestrot, E.M. Krupp, J. Feldmann, *Anal. Bioanal. Chem.,* 2012, **404**, 2185–2191.

41 W.W. Bennett, P.R. Teasdale, J.G. Panther, D.T. Welsh, D.F. Jolley, *Anal. Chem.*, 2011, **83**, 8293-8299.

42 S.N. Ronkart, V. Laurent, P. Carbonnelle, N. Mabon, A. Copin, J-P. Barthélemy, *Chemosphere,* 2007, **66**, 738-745.

43 F.A. Duarte, J.S.F. Pereira, M.F. Mesko, F. Goldschmidt, E.M. de Moraes Flores, V.L. Dressler, *Spectrochim. Acta Part B,* 2007, **62**, 978-984.

44 U. Kohlmeyer, E. Jantzen, J. Kuballa, S. Jakubik, *Anal. Bioanal. Chem.,* 2003, **377**, 6–13.

45 T. Nakazato, H. Tao, T. Taniguchi, K. Isshiki, *Talanta,* 2002, **58**, 121-132.

46 J.A. Day, M. Montes-Bayón, A.P. Vonderheide, J.A. Caruso, *Anal. Bioanal. Chem.,* 2002, **373**, 664-668.

47 L.S. Milstein, A. Essader, E.D. Pellizzari, R.A. Fernando, O. Akinbo, *Environ. Int.,* 2002, **28**, 277-283.

48 A.F. Roig-Navarro, Y. Martines-Bravo, F.J. Lopez, F. Hernández, *J. Chromatogr. A,* 2001, **912**, 319-327.

49 L. G. Sillén, A. E. Martell and J. Bjerrum, *Stability constants of metal-ion complexes*, Chemical Society London, 1964.

50 I. D. Brindle, H. Alarabi, S. Karshman, X. Le, S. Zheng and H. Chen, *Analyst,* 1992, **117**, 407-411.

51 I. Švancara, K. Vytřas, A. Bobrowski and K. Kalcher, *Talanta,* 2002, **58**, 45-55.

Captions of the figures

Fig. 1 Comparison of the retention efficiency between various types of nanoparticles.

Fig. 2 Effect of the Cyst concentration used for capping the thoria nanoparticles on the $As^{(III)}$ retention process.

Fig. 3 Effect of the initial pH of the $As^{(III)}$ sample solution on the $As^{(III)}$ retention process at room temperature for a retention time of 25 min. ($[As^{(III)}]$ = 200 ng mL^{-1}, Amount of the Cyst-capped thoria nanoparticles = 25 mg). The corresponding final pH obtained after finalisation of the retention process is also shown.

Fig. 4 Absolute (A) and relative (B) amount of the $As^{(III)}$ retained as a function of the weight of the Cyst-capped thoria nanoparticles at the optimum pH. Other conditions as in Fig. 3.

Fig. 5 Effect of time on the retention of $As^{(III)}$ by the Cyst-capped thoria nanoparticles at the optimum pH. Other conditions as in Fig. 3. The inset shows the corresponding derivative plot.

Fig. 6 Chromatograms of As(III) and As(V) obtained from arsenic standards solutions (A) and the wash water after centrifugation of the nanoparticles (B).

Supplementary figures

Fig. S1 Plots of the final pH *vs.* the initial pH (A), weight of the Cyst-capped thoria nanoparticles (B), $As^{(III)}$ retention time (C) and the initial $As^{(III)}$ concentrations (D). Other conditions as in Fig. 3.

Fig. S2 Distribution fractions of tartaric acid, cysteine and $As^{(III)}$ species as a function of pH. Note that at the optimum pH, cysteine is mainly present as $HS\text{-}CH_2\text{-}CH(NH_3^+)\text{-}COO^-$, arsenic is as $(HO)_3As$ and tartrate (when present) is as $C_4H_4O_6^{2-}$.

Fig. S3 Plot of the amount of $As^{(III)}$ retained by the Cyst-capped thoria nanoparticles as a function of the initial concentration of $As^{(III)}$ at the optimum pH. Other conditions as in Fig. 3.

Table 1 Instrumental conditions

Plasma	ICP-MS
Rf power (kW)	1.53
Carrier gas flow rate (L min^{-1})	1.05
Makeup gas flow (L min^{-1})	0.15
Measured (*m/z*)	^{75}As
Sampling conditions	
S/C temperature (ºC)	2
Sampling depth (mm)	7.4

Table 2 Values obtained for the theoretical parameters of the two equations (mechanistic and empirical) used to fit the experimental kinetics data (C_o = 200 μg L^{-1})

Mechanistic equation: $\boldsymbol{q = a\left(1 - e^{-b\,t}\right)}$		Empirical equation: $q = \frac{q^t_m\ t}{t_{1/2} + t}$	
Parameter	Values	Parameter	Values
a (μg g^{-1})	82.9±2.0	q^t_m (μg g^{-1})	88.8±1.3
b (μmol L^{-1} min^{-1})	0.28±0.04	$t_{1/2}$ (min)	2.4±0.3
r^2	0.96511	r^2	0.98641

Table 3 Values obtained for the theoretical parameters of the two equations (mechanistic and empirical) used to fit the experimental equilibrium retention data (t = 10 min)

Mechanistic equation: $\boldsymbol{q' = a'\left(1 - e^{-b' C_o}\right)}$		Empirical equation: $q' = \frac{q_m^o C_o}{C_{1/2}^o + C_o}$	
Parameter	Values	Parameter	Values
a' (mg g^{-1})	23.5±0.8	q_m^o (mg g^{-1})	29.0±1.0
b' (dimensionless)	0.02±0.00	$C_{1/2}^o$ (mg L^{-1})	43.0±4.0
r^2	0.98945	r^2	0.99508

Table 4 Parameters obtained for the Langmuir isotherm, ($\frac{1}{q} = \frac{1}{q_m I_L C_e} + \frac{1}{q_m}$), used to model the retention process {C_e (mg L^{-1}): $As^{(III)}$ concentration in the supernatant, q_m (mg g^{-1}): maximum amount of $As^{(III)}$ retained, q (mg g^{-1}): amount of $As^{(III)}$ retained at any time}

Parameter	Value
I_L (L mol^{-1})	120±4
q_m (mg g^{-1})	13.3±2.6
R_L {$=1/(1+I_L C_o)$}	0.01-0.1
r^2	0.97486
ΔG (kJ mol^{-1}) {$= -RT Ln I_L$}	-11.7

Table 5. Comparison of several limits of detection for inorganic arsenic species

Sample	Analytical technique	Limit of detection (calculation)		Reference
		As(III) (μgL^{-1})	As(V) (μgL^{-1})	
Sea water	AuNPs-ETAAS	2.3 (3σ)		19
Sea water	AgNPs-ETAAS	4.4 (3σ)		22
Water/CFA	Bacteria-ICP-MS		0.1 (3σ)	29
Water	AuNPs/CNT-ASV	0.1 (3σ)		31
Urine	μLC-UV-TiO_2NPs/ HG-ICP-MS	0.37 (3σ)	0.22 (3σ)	32
Water	PLA-AuNPs/SPE-ASV	0.09 (S/N = 3)		33
Water	Au(μ/NPs)-C comp-SW-ASV	0.4 (3σ)		34
Water	HPLC-ICP-MS	0.19 (3σ)	0.52 (3σ)	35
Water	(MEA/Au)-DP-ASV	0.02 (3σ)		36
Water	CNTs-ETAAS	0.02 (3 standard error of regression)		37
Water	μAu electrode/CSV	0.04 (3σ)		38
Rice, tuna fish, wheat	HPLC-ICP-MS	0.05 (S/N = 3)		39
Sea food	HPLC-HG-ICP-MS	0.0004 mg Kg^{-1} (3σ)		40
Sea water	M-Si-DGT-ICP-MS	0.03 (σ changed by DGT equation)		41
Water	HPLC-ICP-MS	0.017 (5σ)	0.026 (5σ)	42
Industrial water	LC-ICP-MS	0.02 (3σ)	0.10 (3σ)	43
Marine biota	IC-ICP-MS	0.008 (DIN 32645)		44
Sea water	LC-ICP-MS	0.015 (3σ)	0.012 (3σ)	45
	LC-ICP-ORS-MS	0.025 (3σ)	0.020 (3σ)	
	LC-HG-ICP-MS	0.0028 (3σ)	0.0045 (3σ)	
Drinking water	LC-ICP-MS	0.067 (3.14σ)	0.089 (3.14σ)	46
Drinking water	IEC-ICP-MS	0.09 (3σ)	0.3 (3σ)	47
Surface water	HPLC-ICP-MS	0.046 (3σ)	0.03 (3σ)	48
Aqueous solutions	ThNPs-ICP-MS	0.07 (3σ)	0.07 (3σ)	This work

NPs: Nanoparticles; CNT: Carbon nanotubes; PLA: poly(L-lactite); SPE: Screen-printed carbon electrode; SW-ASV: Square-wave anodic striping voltammetry; CSV: cathodic striping voltammetry; M-Si-DGT: mercapto-silica-diffusive gradients in thin films; (MEA/Au)-DP-ASV: mercapto ethylamine modified gold electrode-differential pulse anodic striping voltammetry; IEC: ion-exchange chromatography; HPLC-ICP-MS=Liquid chromatography inductively coupled plasma mass spectrometry; LC-ICP-ORS-MS=Liquid chromatography inductively coupled plasma mass spectrometry using reaction cell; LC-HG-ICP-MS=Liquid chromatography inductively coupled plasma mass spectrometry using hydride.

Table 6 Spiking studies and accuracy of the developed method (n = 3)

Sample	Content (ng mL^{-1})	Added (ng mL^{-1})	Found (ng mL^{-1})	Recovery (%)
Deionized water	-	10	10.2±0.4	102.0
		50	49.6±0.7	99.2
		100	102.6±0.8	102.6
		200	195.4±0.8	97.7
	Content (ng mg^{-1})	Added (ng mg^{-1})	Found (ng mg^{-1})	Recovery (%)
NIST SRM 1633a	145±15	0	150±10	103.4
		50	197±8	101.0
		100	247±7	100.8
		200	346±5	100.3
NIST SRM 1568a	0.29±0.03	0	0.30±0.04	103.5
		2	2.30±0.05	100.4
		5	5.20±0.08	98.3
		10	10.22±0.08	99.3

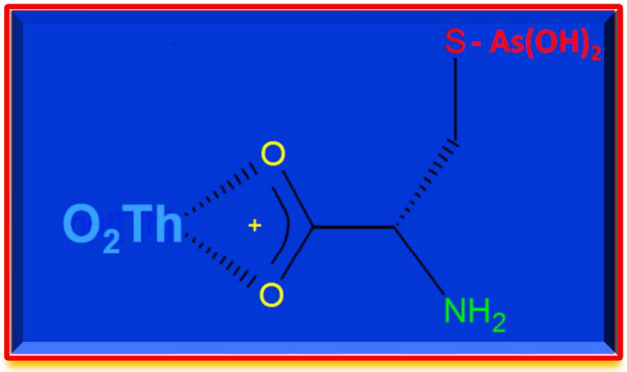

Cysteine-capped thoria nanoparticles resulted to be an excellent material for retention of arsenite and arsenate from aqueous solutions.

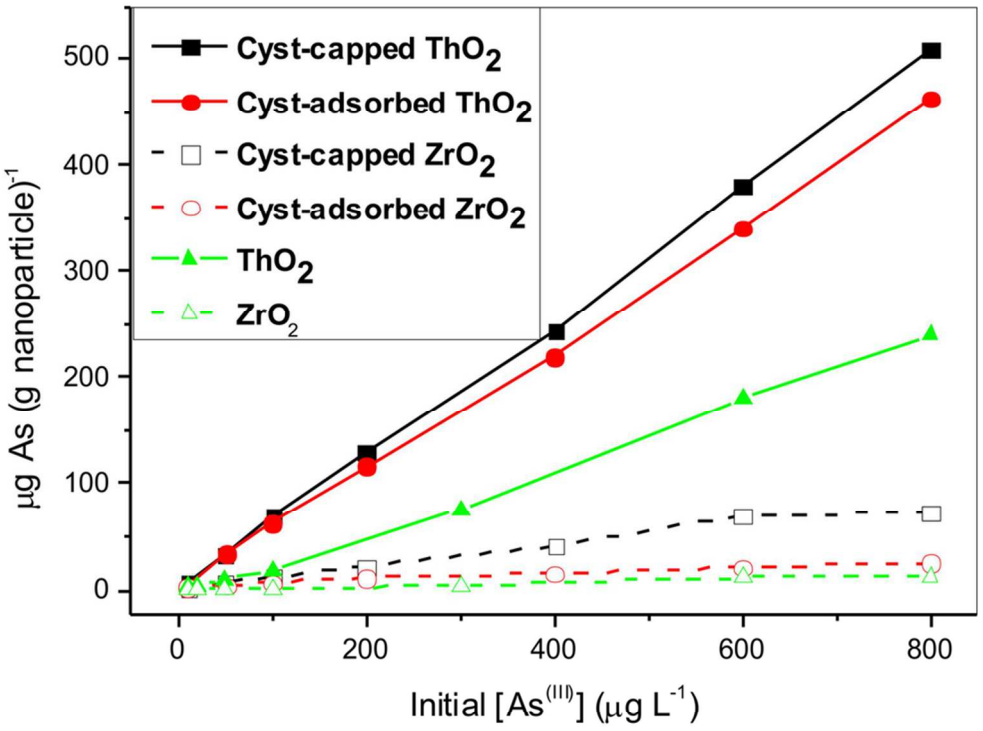

85x85mm (300 x 300 DPI)

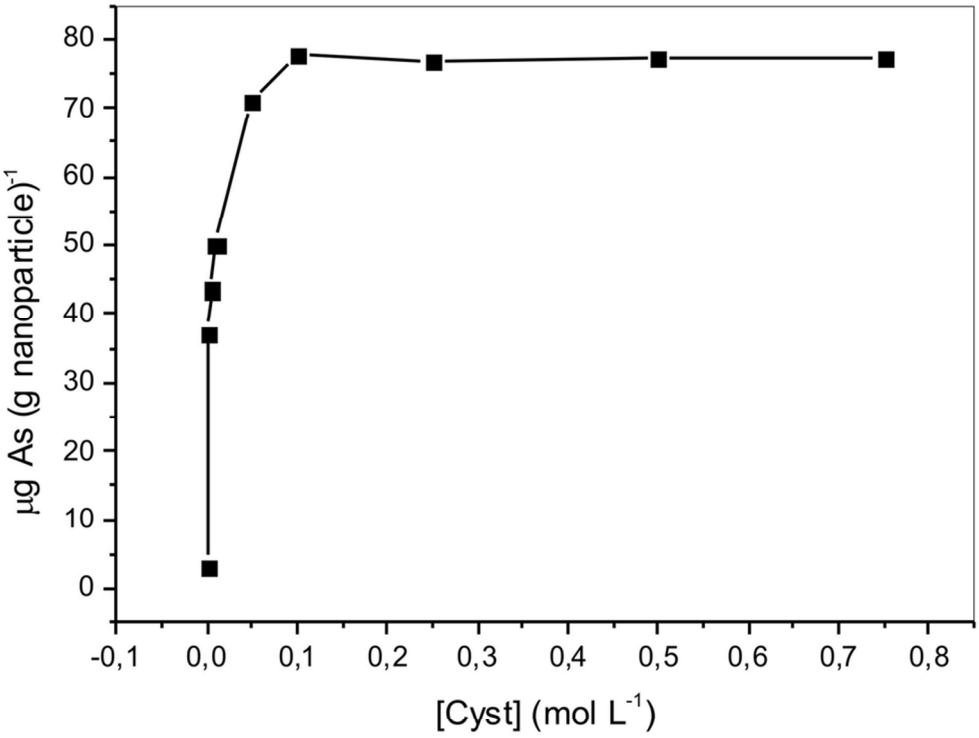

85x85mm (300 x 300 DPI)

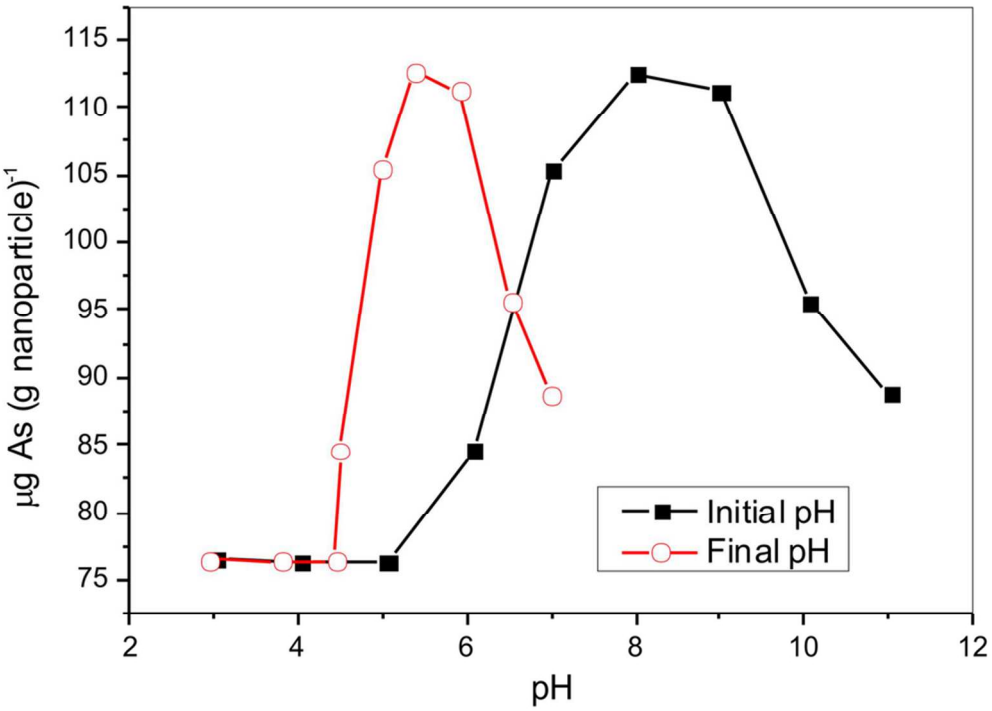

85x85mm (300 x 300 DPI)

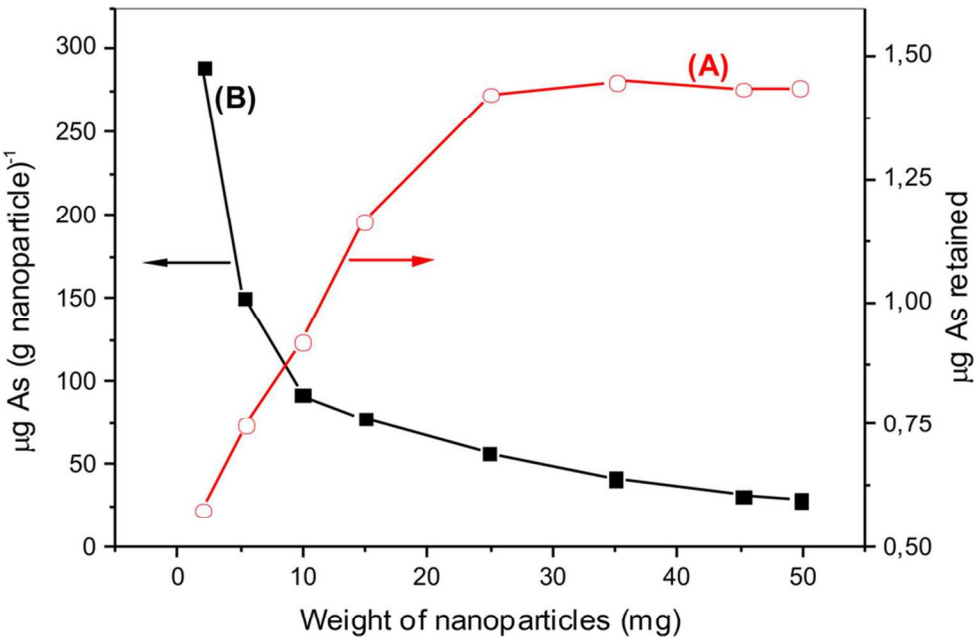

85x85mm (300 x 300 DPI)

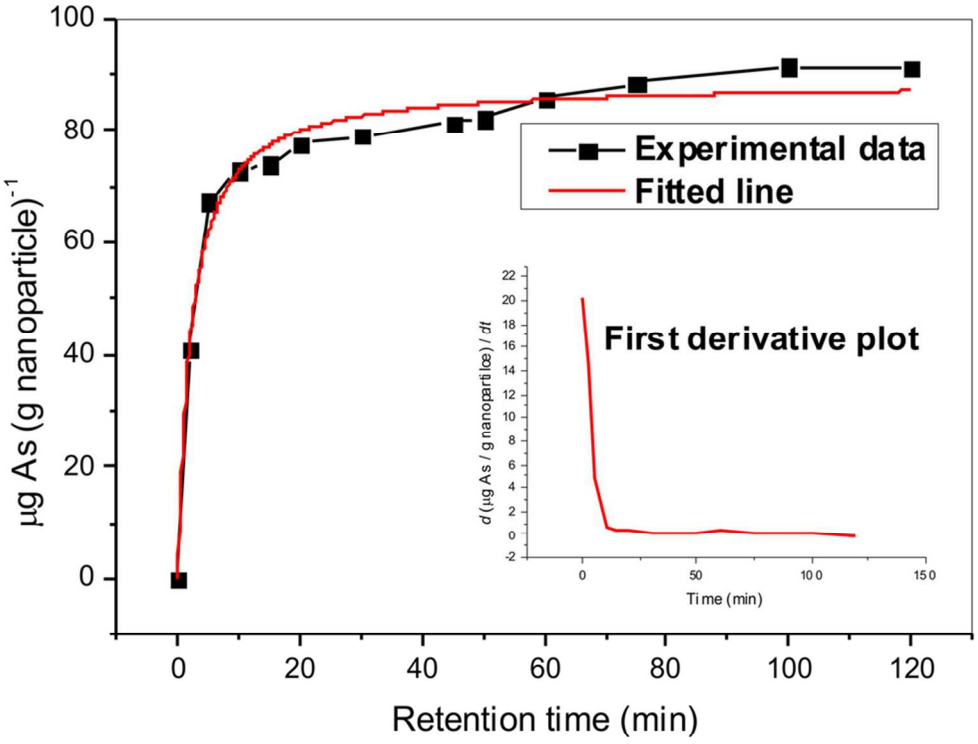

85x85mm (300 x 300 DPI)

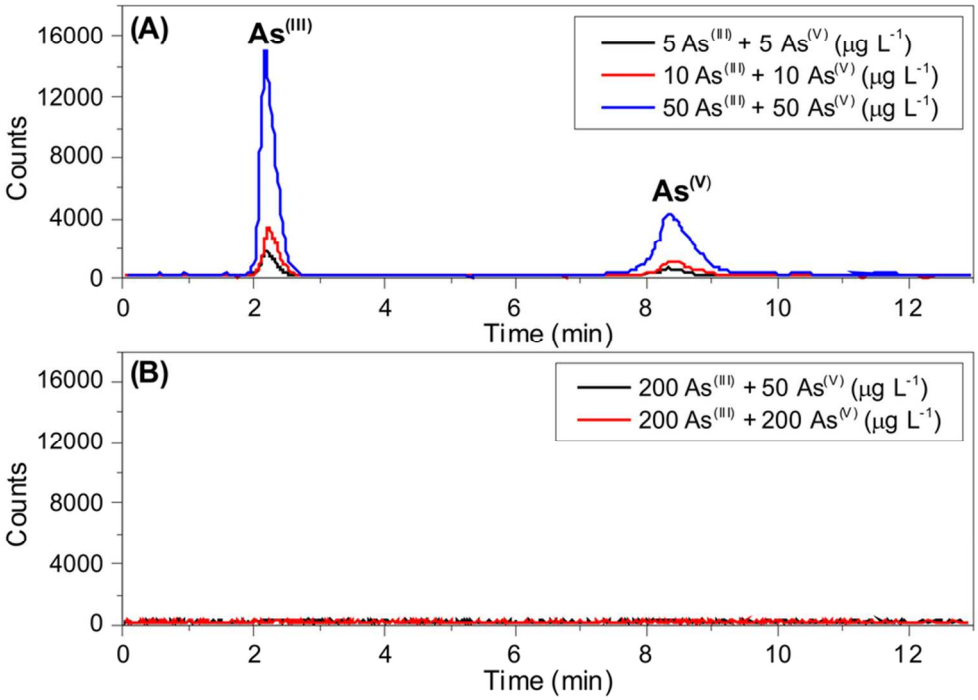

85x85mm (300 x 300 DPI)